Sensors **2015**, *15*, 1-x manuscripts; doi:10.3390/s150x0000x

OPEN ACCESS

sensors

ISSN 1424-8220

www.mdpi.com/journal/sensors

Article

Inertial Sensing Based Assessment Methods to Quantify the Effectiveness of Post-Stroke Rehabilitation

Hsin-Ta Li [1], Jheng-Jie Huang [1], Chien-Wen Pan[2], Heng-I Chi [1] and Min-Chun Pan [1,3,*]

[1] Graduate Institute of Biomedical Engineering, National Central University, Jhongli 320, Taiwan; E-Mails: winterfrost1143@gmail.com, d0785208@hotmail.com, nocilole@hotmail.com

[2] Hsinchu Air Base, Hsinchu City 300, Taiwan; E-Mail: kkpan535634@gmail.com

[3] Department of Mechanical Engineering, National Central University, Jhongli 320, Taiwan; E-Mail: pan_minc@cc.ncu.edu.tw

***** Author to whom correspondence should be addressed; E-Mail: pan_minc@cc.ncu.edu.tw; Tel.: +886-3-4267312; Fax: +886-3-4254501.

Academic Editor:

Received: / Accepted: / Published:

Abstract: In clinical settings, traditional stroke rehabilitation evaluation methods are scored by occupational therapist subjectively, and the variation of assessment results depends on individual directly. To the other end, this study employed inertial measurement units to construct stroke rehabilitation assessment system. The inertial signals from upper extremity were acquired, and extracted three quantitative indicators to reflect rehabilitation performance during stroke patients' movement examination, i.e. shoulder flexion. Therefore, an objective quantitative evaluation system was developed. Both healthy adults and stroke patients were recruited to investigate the correlation between the proposed quantitative evaluation indices and traditional rehab assessment scales. Especially, the weighting for each of three evaluation indices was estimated by the least squares method through the correlation between the indices and traditional assessment scales. The quantitative results demonstrate the proposed method enables to accurately reflect patients' recovery from pre-rehabilitation, and confirm the feasibility of applying inertial signals to evaluate rehab performance. The implemented assessment scheme appears to have the potential to overcome some of the shortcomings of traditional assessment methods and indicate rehab performance correctly.

Keywords: inertial measurement; stroke rehabilitation evaluation; quantitative assessment scale.

1. Introduction

According to the World Health Organization (WHO), stroke was the second leading causes of death in the world [1]. There are about 17 million stroke people in 2010 [2] and three-fourth of survivors were affected by stroke and became disable [3] due to the deteriorated cerebrovascular. Research showed that repetitive exercises training may be beneficial to stroke for ameliorating their daily movement [4] and help patients recover. Therefore. Post-stroke rehabilitation treatments are indispensable for patients.

In clinical, classical assessment methods typically include Fugl-Meyer Assessment (FMA) [5], Wolf Motor Function Test (WMFT) [6] and Upper Extremity Performance Evaluate Test for the Elderly (TEMPA) [7], and other Likert-type assessment scales. Although traditional assessment scales have been used for many years and the evaluation results are accepted widely in various fields, they are scored by occupational therapist subjectively. The variations of assessment results depend on individual directly. Furthermore, Likert-type scales give scale scores based on numerical ranges. Thus, an individual case's score between two scales may be inaccurate to describe the rehabilitation result. It appears that classical assessment methods may be short of an objective standard for evaluating the effectiveness of stroke rehabilitation.

To address these problems, it is nontrivial to develop objective and quantitative assessment methods during the rehabilitation treatment. Many researches [8-11] were designated to analyze human upper-extremity motion as upper limbs are frequently used in daily life [12]. Therefore, this study focus on the recovery of upper limb motion primarily. Inertial sensors were applied for rehabilitation engineering successfully; for instance, researchers proposed position-sensing technology to construct tele-rehabilitation system [13], and some others combined inertial sensors with ZigBee wireless transmission to measure and reconstruct motion trajectory [14-15]. Evidences showed that inertial sensors are able to provide the accurately quantified information of human motion [16]. As a result, this study employs nine-axis inertial measurement units to construct a stroke rehabilitation assessment system. We intend to reflect rehabilitation performance during stroke patients' movement exam and quantitatively assess the rehabilitation performance.

2. Inertial measurement system

An Inertial Measurement Unit (IMU) exploits the dynamic behavior resulting from inertial force acting on an object. The basic dynamic parameters are acceleration and angular velocity along specific axes. An Inertial measurement system includes magnetometers, accelerometers, and gyroscopes to measure magnetic field, linear acceleration, and angular velocity separately for the orientation evaluation of a body to be measured in 3-D space.

The aim of this study is to assess effectiveness of post-stroke rehabilitation via inertial signals from stroke patients. For this purpose, we design a wireless inertial sensing device shown in Figure 1 that integrates inertial sensors and a control module that connected to a circuit to display wireless transmission of signals in real time by a user interface in a personal computer. The following paragraphs introduce the elements of this measuring device.

Figure 1. Appearance of inertial measuring device. Dimensions: 7.3×5.4×4.3 cm. Approximate weight with batteries: 125 g.

2.1. Hardware

2.1.1. Inertial Sensing Module - MPU-6050 EVB

The inertial sensing module used in this study is MPU-6050 Evaluation Board (EVB, lnvenSense®). This evaluation board consists of a 3-axis magnetometer (AsahiKASEI®) and a MPU-6050 module (InvenSense®) which combines a 3-axis gyroscope and a 3-axis accelerometer. The module features a user-programmable full-scale range of accelerometer and gyroscope to fit different precision of motion. This module is used to acquire the inertial signals of motion. Parameter setting and specification are shown in Table 1 [17-18]. The sampling rate is set to 50 Hz, the full scale range of the accelerometer is set to ±4 G, and the full scale range of gyroscope is ±2000 dps for measuring limb motion.

2.1.2. Control Module (SIOC) - Based on STM32F103C8T6

The STM32F103C8T6 is a programmable microcontroller manufactured by STMicroelectronics® featuring ARM 32-bit Cortex™-M3 CPU Core with 72 MHz maximum frequency. To receive data from sensing module and transmit data to wireless transmission module, this microcontroller was selected to implement communications protocol, parameter setting and data acquiring.

2.1.3. Wireless Transmission Module - XBee

The advantage of ubiquitous computing and the proliferation of portable computing devices have raised the importance of mobile and wireless networking. Recently tremendous interest have drawn broadband wireless access system, including wireless local area networks (WLANs), broadband wireless access, and wireless personal networks (WPANs) [19].

Zigbee is the architecture on top of the IEEE 802.15.4 reference stack model and takes full advantage of its powerful physical radio layers. IEEE 802.15.4 is hence a low-rate wireless personal area network solution. It designed to be simple for low-power devices and light weight wireless networks. Zigbee technology enables the coordination of communication among thousands of tiny sensors, which are very low cost, with lower power consumption and low data rate. These benefits are suitable for physiological signal measurement. XBee [20] is a wireless transmission module (Digi®), and its specification is shown in Table 2. This module is used to receive data from control module and transmit data to PC.

		Parameter	Conditions	Min	Typical	Max	Unit
MPU-6050		Voltage Range		2.375		3.46	V
		Temperature Range		-40		85	°C
		Sample Rate			50		Hz
	Gyroscope	Full-Scale Range	FS_SEL=3		±2000		°/s
		ADC Word Length			16		Bits
		Sensitivity Scale Factor	FS_SEL=3		16.4		$\frac{LSB}{°/s}$
		Initial Calibration Tolerance	25 ° C	-3		3	%
		Nonlinearity	25 ° C		0.2		%
		Initial Zero-Rate Output Tolerance	25 ° C		±20		°/s
	Accelerometer	Full-Scale Range	AFS_SEL=1		±4		g
		ADC Word Length			16		Bits
		Sensitivity Scale Factor	AFS_SEL=1		8192		LSB/g
		Initial Calibration Tolerance		-3		3	%
		Nonlinearity	25 ° C		0.5		%
		Cross Axis Sensitivity		-2		2	%
		Zero-g Offset	X & Y axes	-35		35	mg
			Z axis	-60		60	mg
AK8975	Magnetometer	Voltage Range		2.4	3	3.6	V
		Temperature Range		-30		85	°C
		ADC Word Length			13		Bits
		Measurement Range			±1229		μT
		Sensitivity Scale Factor			0.3		μT/LSB
		Magnetic Sensor Initial Offset		-1000		1000	LSB
		Sample Rate			50		Hz

Table 1. Parameter setting and specification of MPU-6050.

Outdoor RF line-of-sight Range	Up to 90m
RF Data Rate	250Kbps
Supply Voltage	2.8V-3.4V
Operating Frequency	ISM 2.4GHz
Dimensions	2.438cm×2.761cm
Operating Temperature	-40 to 85 ºC
Number of Channels	16

Table 2. Specification of XBee.

2.2. Software

The software is designed to store data, calibrate device and display inertial signals in real time. This user interface which was developed in LabVIEW® (National Instrument, NI®), includes nine monitors to demonstrate the inertial sensing signals of this inertial measuring system, showing information of acceleration, angular velocity and magnetics separately. Control panels are used to calibrate accelerometer, gyroscope and magnetometer sensor and record sensing signals. In addition, it allows one to select the number of times to record and view.

2.3. Common Error Model of Inertial Measurement Device

Imperfections of the sensors may result in various errors in measurement. To compensate and calibrate a sensor, building an error model is necessary. In this section we introduce some common errors of accelerometers, gyroscopes, and magnetometers, and build the error models.

2.3.1. Errors of Accelerometer and Gyroscope

Some common errors of accelerometers and gyroscopes [21], are
(a) bias, which is any nonzero sensor output when the input is zero;
(b) scale factor error, often resulting from aging or manufacturing tolerances;
(c) nonlinearity, which is presented in most sensors in some degree;
(d) asymmetry, often from mismatched push-pull amplifiers;
(e) dead zone, usually due to mechanical friction or lock-in; and
(f) quantization error, inherent in all digital systems

For a cluster of three gyroscopes or accelerometer with nominally orthogonal input axis. The effects of individual scale factor deviations and input axis misalignments from their nominal values can be modeled by

$$\vec{\mathrm{Z}}_{output} = S_{nominal}(I + M)\vec{\mathrm{Z}}_{input} + \vec{\mathrm{b}}_Z, \tag{1}$$

where $\vec{\mathrm{Z}}_{input}$ and $\vec{\mathrm{Z}}_{output}$ are the sensed values (accelerations or angular velocities), $S_{nominal}$ is the nominal sensor scale factor, $\vec{\mathrm{b}}_Z$ means the bias of sensor, and M is the matrix which represents the scale factor deviations and input axis misalignments. Equation (1) is in "error form," where the corresponding "compensation from" is

$$\vec{\mathrm{Z}}_{input} = \frac{1}{S_{nominal}}(I + M)^{-1}(\vec{\mathrm{Z}}_{output} - \vec{\mathrm{b}}_Z),$$

$$\vec{\mathrm{Z}}_{input} = \frac{1}{S_{nominal}}(I - M + M^2 - M^3 + \cdots)(\vec{\mathrm{Z}}_{output} - \vec{\mathrm{b}}_Z). \tag{2}$$

If the misalignments and scale factor deviations are sufficiently small, Eq. (2) can be approximate to

$$\vec{\mathrm{Z}}_{input} \approx \frac{1}{S_{nominal}}(I - M)(\vec{\mathrm{Z}}_{output} - \vec{\mathrm{b}}_Z). \tag{3}$$

The compensation form is the one used in system implementation for compensating sensor output using a single constant matrix $\overline{\mathrm{M}}$ in the from

$$\bar{\mathrm{M}} \equiv \frac{1}{S_{nominal}}(I+M)^{-1} \approx \frac{1}{S_{nominal}}(I-M). \tag{4}$$

Then,

$$\vec{\mathrm{Z}}_{input} = \bar{\mathrm{M}}(\vec{\mathrm{Z}}_{output} - \vec{\mathrm{b}}_Z). \tag{5}$$

Using Eq. (5), the compensation form of gyroscope is written as

$$\vec{\omega}_{input} = \bar{\mathrm{M}}_{gyro}(\vec{\omega}_{output} - \vec{\omega}_{bias}), \tag{6}$$

and the compensation form of accelerometer as

$$\vec{\mathrm{a}}_{input} = \bar{\mathrm{M}}_{accelerometer}(\vec{\mathrm{a}}_{output} - \vec{\mathrm{a}}_{bias}). \tag{7}$$

2.3.2. Errors of Magnetometer

The errors of a magnetometer comes from the magnetic distortions [22]. Distortion of the earth's magnetic field are the results of external magnetic influences generally classified as either hard or soft iron effect. If no distorting effects are presented, rotating a magnetometer through a minimum 360 degree and plotting the result data as y-axis versus x-axis will result in a circle centered around (0, 0).

Hard iron distortion is produced by materials that exhibit a constant, additive distortion to the earth's magnetic field. This distortion makes an offset of the origin of the ideal circle from (0, 0), as shown in Figure 2(a). Compensating for hard iron distortion is straightforward, accomplished by determining the offsets and then applying them directly on the data. The compensation model of the hard iron distortion is given by

$$\begin{bmatrix} \mathrm{B}_{i,input} \\ \mathrm{B}_{j,input} \\ \mathrm{B}_{k,input} \end{bmatrix}_{hard} = \left(\begin{bmatrix} \mathrm{B}_{i,output} \\ \mathrm{B}_{j,output} \\ \mathrm{B}_{k,output} \end{bmatrix} - \vec{\mathrm{B}}_{hard} \right), \tag{8}$$

where B_{input} is the corrected magnetic vector, B_{output} is the magnetic vector with hard iron distortion, and the matrix $\vec{\mathrm{B}}_{hard}$, the compensation matrix, is given by

$$\vec{\mathrm{B}}_{hard} = \begin{bmatrix} \mathrm{B}_{i,hard} \\ \mathrm{B}_{j,hard} \\ \mathrm{B}_{k,hard} \end{bmatrix} = \begin{bmatrix} \frac{(\mathrm{B}_{i,max}+\mathrm{B}_{i,min})}{2} \\ \frac{(\mathrm{B}_{j,max}+\mathrm{B}_{j,min})}{2} \\ \frac{(\mathrm{B}_{k,max}+\mathrm{B}_{k,min})}{2} \end{bmatrix}. \tag{9}$$

Soft iron is similar in nature to hard iron distortion in that it is also additive to the earth's magnetic field. However, the distortion produced by soft iron materials is dependent upon the orientation of the material with the earth's field. This distortion is typically exhibited as a perturbation of the ideal circle into an ellipse, as shown in Figure 2(b). Identifying θ in Figure 2(b) is completed by using Eq. (10) to calculate the line segment r shown like

$$r = \sqrt{x^2 + y^2}. \tag{10}$$

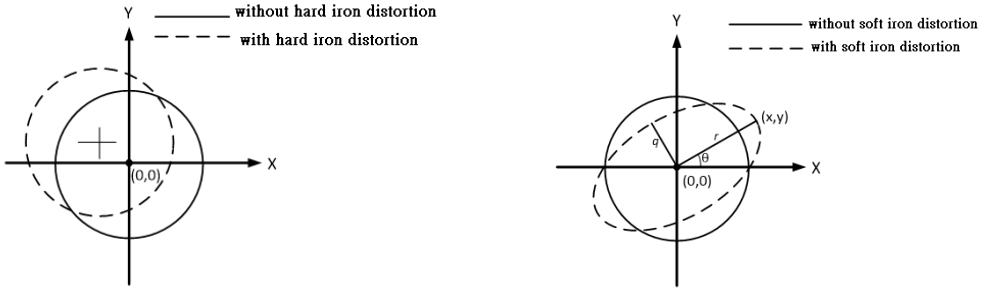

(**a**) (**b**)

Figure 2. (**a**) Hard iron distortion. (**b**) Soft iron distortion.

After calculating all the magnitude of each point on the ellipse, we identified the maximum magnitude of computed values, and the coordinates of this value will correspond with the major axis. Once θ has been identified, rotating points on the ellipse and making the major axis be aligned with the x-axis, the minor axis be aligned with y-axis, then defining a scale factor σ as

$$\sigma = \frac{\mathrm{q}}{r}, \tag{11}$$

where q is the magnitude of the minor axis, and r is the magnitude of the major axis.

Once the scale factor σ has been obtained, each x-value from magnetometer is then divided by this scale factor to produce the desired circle. For a cluster of three magnetometers, the compensation model of the soft iron distortion is given by

$$\begin{bmatrix} \mathrm{B}_{i,input} \\ \mathrm{B}_{j,input} \\ \mathrm{B}_{k,input} \end{bmatrix}_{soft} = \sigma M \begin{bmatrix} \mathrm{B}_{i,output} \\ \mathrm{B}_{j,output} \\ \mathrm{B}_{k,output} \end{bmatrix}, \tag{12}$$

where B_{input} is the corrected magnetic vector, B_{output} is the magnetic vector with soft iron distortion, and the matrix M denotes the rotation matrix written as

$$M = \mathrm{R}_z \mathrm{R}_y \mathrm{R}_x, \tag{13}$$

where

$$\mathrm{R}_x = \begin{bmatrix} 1 & 0 & 0 \\ 0 & cos\theta_x & -sin\theta_x \\ 0 & sin\theta_x & cos\theta_x \end{bmatrix},$$

$$\mathrm{R}_y = \begin{bmatrix} cos\theta_y & 0 & sin\theta_y \\ 0 & 1 & 0 \\ -sin\theta_y & 0 & cos\theta_y \end{bmatrix}, \text{ and} \tag{14}$$

$$\mathrm{R}_z = \begin{bmatrix} cos\theta_z & -sin\theta_z & 0 \\ sin\theta_z & cos\theta_z & 0 \\ 0 & 0 & 1 \end{bmatrix}.$$

Combining (8) and (12), the compensation model of the magnetometer can be written as

$$\begin{bmatrix} \mathrm{B}_{i,input} \\ \mathrm{B}_{j,input} \\ \mathrm{B}_{k,input} \end{bmatrix} = \sigma M \left(\begin{bmatrix} \mathrm{B}_{i,output} \\ \mathrm{B}_{j,output} \\ \mathrm{B}_{k,output} \end{bmatrix} - \vec{\mathrm{B}}_{hard} \right) \quad (15)$$

2.4. Device Calibration

Before using the device to measure signals, all sensors of the device need to be calibrated, and this section will discuss the method to compensate errors.

2.4.1. Gyroscope

The main error of the gyroscope is bias. According to Table 1, the initial zero-rate output tolerance of the gyro is ±20 dps. To compensate the error, we place sensor on the platform and measuring the bias, then estimating the average of bias and subtracting the bias from the sensing data. The flow diagram of gyroscope calibration illustrated in Figure 3(a) and the result of calibration shows in Figure 4(a).

2.4.2. Accelerometer

The accelerometer needs to compensate the bias error and scale factor error. The calibration of bias and scale factor can be achieved by measuring gravity acceleration [23]. When the axis of accelerometer align with the direction of gravity, the sensor will detect gravity acceleration as 1 G. We can obtain the bias by aligning both positive and negative axes to the gravity direction and measuring the gravity acceleration a_{+G} and a_{-G}, then estimating the bias with using

$$a_{bias} = \frac{a_{+G}+a_{-G}}{2}. \quad (16)$$

This two parameters can also be used to estimate the scale factor $\bar{M}_{acc}$ by

$$\bar{M}_{acc} = \left(\frac{a_{+G}-a_{-G}}{2}\right)^{-1}. \quad (17)$$

The flow diagram of accelerometer calibration illustrated in Figure 3(b) and the result of calibration shows in Figure 4(b).

2.4.3. Magnetometer

To calibrate the magnetometer, the distortion of hard and soft iron need to be solved. Both of the distortion can be compensated by measuring the magnetic field of earth. The calibration flow diagram of magnetometer illustrated in Figure 3(c). Rotating magnetometer 360° around three axes will make one know the magnetic field distribution of earth. After obtaining the magnetic field distribution, the distortion of both hard iron and soft iron can be calibrated. The calibration result of magnetometer is shown in Figure 4(c).

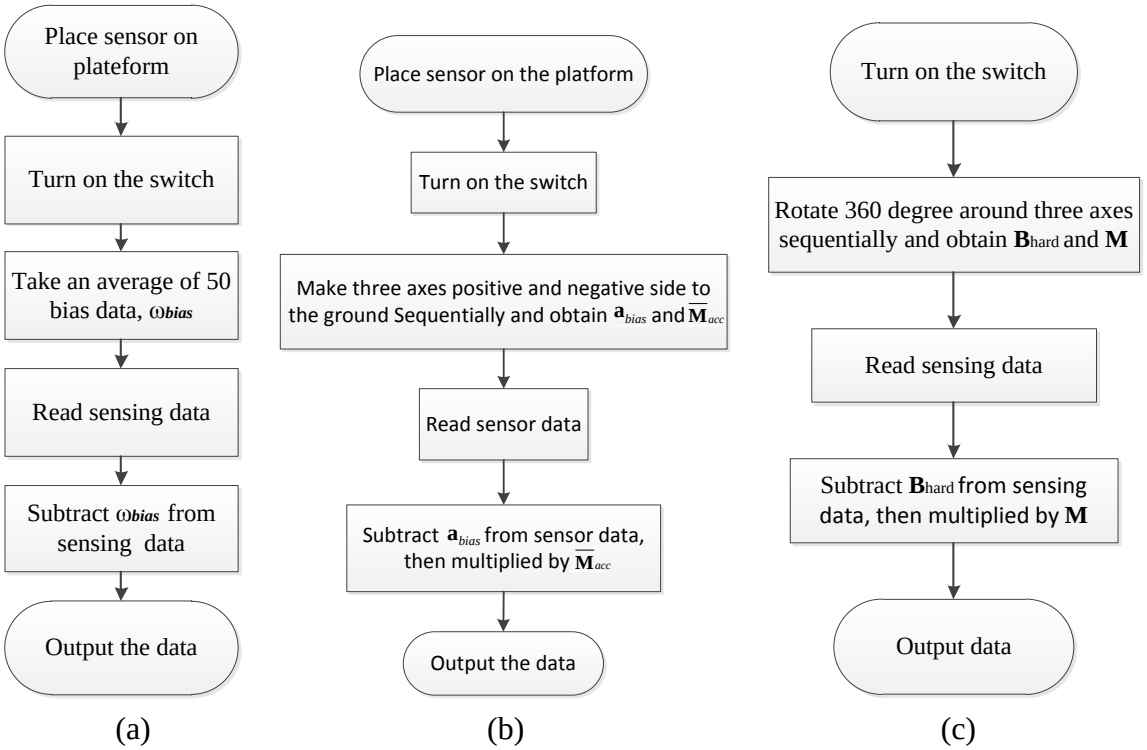

Figure 3. Flow diagram of device calibration. Display of calibration processes of (a) gyroscopes, (b) accelerometers, and (c) magnetometers, respectively.

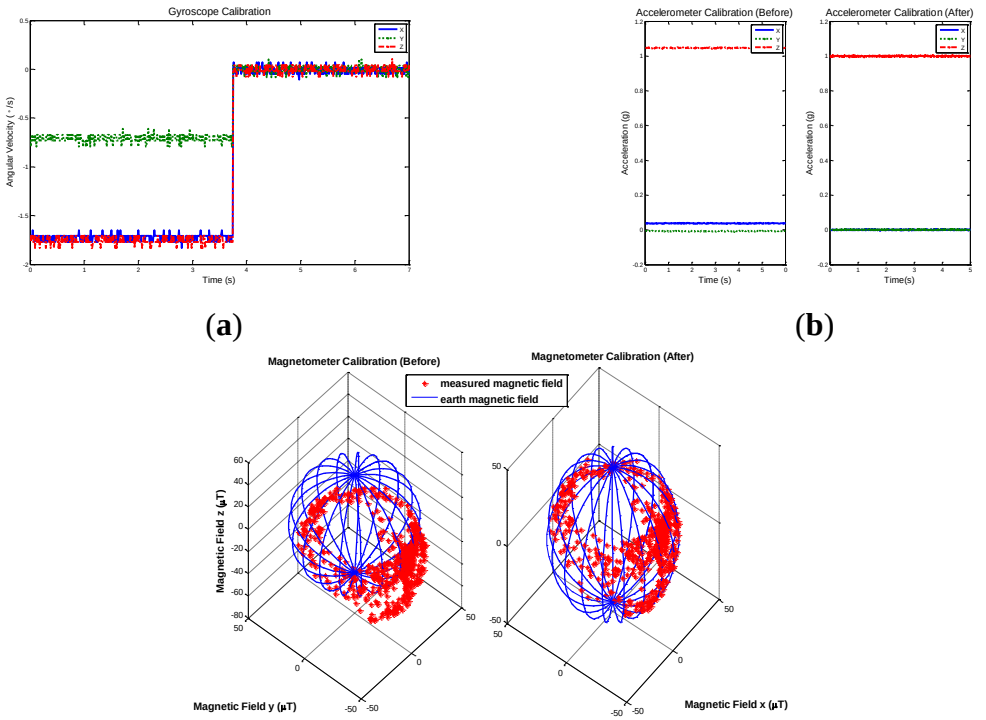

Figure 4. Calibration result. Display of the calibration results of (a) gyroscopes, (b) accelerometers, and (c) magnetometers, respectively.

3. Post-Stroke Rehabilitation Assessment Method

The previously mentioned inertial measurement system was applied to acquire the inertial signals, which are from stroke patients before and after rehabilitation. In order to assess treatment results, inertial information is used to quantify the effectiveness of post-stroke rehabilitation. The following of this section will depict the detail of assessment method.

3.1. Experiment Protocol

Clinically, after post-stroke rehabilitation treatments, therapies will design some testing movements such as "shoulder flexion", of which is simpler than some rehabilitation training or daily upper-limb movements. As a result, this study takes "shoulder flexion" as the movement to assess the rehabilitation effectiveness. The complete motion of shoulder flexion is depicted as following:

The initial position is hand hanging down with palm backward naturally. While motion is occurring, the arm is straightly uplifted approximately 180 degrees, until the arm is directly overhead, and end with the arm dropped down to initial position. One such movement is called shoulder flexion, in which the arm is lifted vertically in front of the body in a forward direction.

During assessment, the subjects were required to sit on chair and lift arm as high as possible. In this experiment, the patients will execute the movement 80 times repeatedly, with two minutes rest for every ten times of motion.

The position of sensors in this experiment is demonstrated in Fig. 5. In order to measure the inertial signals from forearm, upper arm and shoulder, the subject's wrist, elbow and shoulder was placed with sensors. Notice that the coordinate systems of accelerometer and gyro are defined differently.

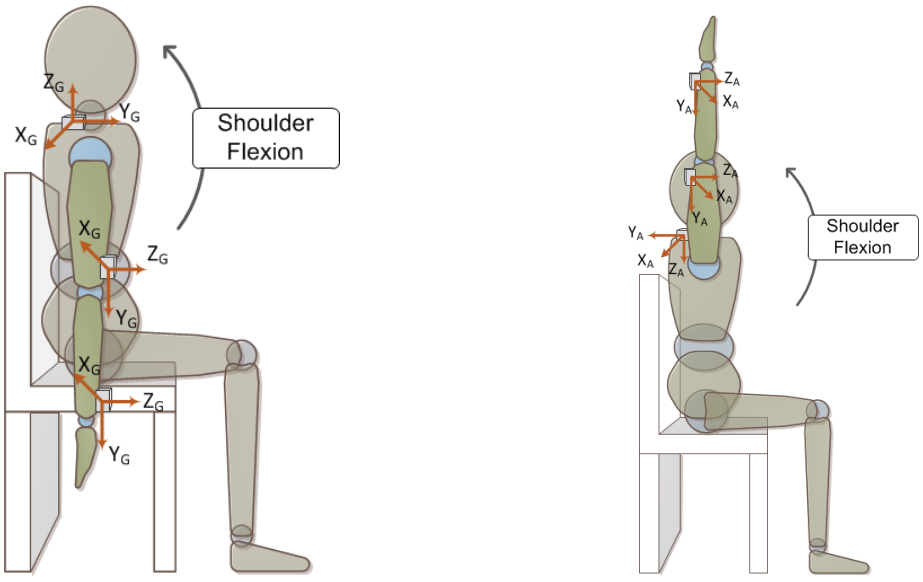

(**a**) (**b**)

Figure 5. Illustration of sensors' placement and assessment motion. (**a**) Display the initial position of shoulder flexion and motion direction. 3-axis direction of gyro was marked, expressing by subscript 'G'. (**b**) Display the end position of shoulder flexion. 3-axis direction of accelerometer was marked, expressing by subscript 'A'.

3.2. Traditional Assessment Method

To evaluate patient's rehabilitation, the therapist will give a score based on their implementation status. In other words, when the patient performs the specified action of the test, the therapist will give a corresponding assessment to the project according to the actual condition of the patient's movement. The criterions of clinical evaluation are as follows:

1. Elevation (or bending) angle: the closer to unaffected side, the better it is.
2. Synergy: the less unnecessary actions, the better it is.
3. Action execution speed: the closer to unaffected side, the better it is.

3.3. The Objective and Quantitative Assessment Indicators

Because the WMFT scale is one of the Likert-type scales [24], and the scale ranging 0–5 which makes WMFT only represent a rough motion status. Additionally, the traditional assessment scales exist subjective judgments depended on therapists. In order to evaluate patients quantitatively and objectively, this study design assessment indicators consulted from clinical evaluation.

3.3.1. The ratio of Y-axis maximum acceleration on wrist of affected side to unaffected

With the elevate angle becomes large, Y-axis acceleration will increase from -1 G to + 1 G. Based on this observation, this study using the ratio of Y-axis maximum acceleration on wrist of affected side to unaffected side to construct the indicator for elevation angle. Its mathematical definition can be defined as

$$A_{2,r} = \frac{A_{2y,max}+1}{A_{2yn,max}+1}, 0 \le A_{2,r} \le 1, \quad (18)$$

where $A_{2y,max}$ is the Y-axis maximum acceleration of affected side and $A_{2yn,max}$ is the Y-axis maximum acceleration of unaffected side, subscript "2" denotes the sensor on elbow. The larger the $A_{2,r}$ is, the closer the elevation angle of affected side is to the unaffected side.

3.3.2. The proportion of X-axis angular velocity to three-axis angular velocity

In ideal motion of shoulder flexion, it can be simply described as the movement that arm rotates with X-axis while Y-axis and Z-axis direction around shoulder as the fulcrum. That is, the measured Y-axis and Z-axis signals by inertial sensors can be viewed as unnecessary movements. Via this relationship, this study calculates the proportion of X-axis angular velocity's root mean square to the summation of three-axis angular velocity's root mean square as the quantitative assessment parameters for synergy indicator. The root mean square of angular velocity is defined as

$$G_{ij,rms} = \frac{1}{T}\int_T G_{ij}(t)dt \ , i = 1,2;\ j = x, y\ or\ z, \quad (19)$$

where $G_{ij}(t)$ denotes the gyro signal, i=l represents the sensor on wrist and i=2 represents the sensor on elbow, and j represents axis direction.

And the quantitative assessment parameters is defined as

$$G_{1,p} = \frac{G_{1x,rms}}{G_{1x,rms} + G_{1y,rms} + G_{1z,rms}}, 0 \le G_{1,p} \le 1$$
$$G_{2,p} = \frac{G_{2x,rms}}{G_{2x,rms} + G_{2y,rms} + G_{2z,rms}}, 0 \le G_{2,p} \le 1 \quad (20)$$

where $G_{1,p}$ is the quantitative assessment parameter on wrist and $G_{2,p}$ is the quantitative assessment parameter on elbow.

To construct the indicator for synergy, we calculate the ratio of the average of quantitative assessment parameters both on wrist and elbow of affected side to unaffected:

$$G_r = \frac{G_{1,p} + G_{2,p}}{G_{1n,p} + G_{2n,p}}, 0 \le G_r \le 1 \quad (21)$$

where $G_{1n,p}$ and $G_{2n,p}$ represent the quantitative assessment parameter on wrist and elbow of unaffected side, respectively. The meaning of this assessment indicator for synergy, G_r , is the ratio of the unnecessary action generated by executing shoulder flexion between affected side and unaffected side. The larger G_r is, the closer to unaffected side the degree of synergy will be.

3.3.3. The difference of motion execution time between affected side and unaffected

Due to the elevation angle between affected and unaffected side are different, it cannot express the difference of elevation angle merely comparing the motion execution time between affected and unaffected side. As a result, to objectively assess the difference of motion execution time between affected side and unaffected, this study calculates the ratio of Y-axis maximum acceleration on wrist to motion execution time as the execution time parameters, $T_{r,affected}$ and $T_{r,normal}$

$$T_{r,affected} = \frac{1}{N}\sum_{i=1}^{N}\frac{A_{2y,max} + 1}{t_{affected,i}}$$
$$T_{r,normal} = \frac{1}{M}\sum_{i=1}^{M}\frac{A_{2yn,max} + 1}{t_{normal,i}} \quad (22)$$

where $A_{2y,max}$ and $A_{2yn,max}$ represent the Y-axis maximum acceleration on wrist for affected and unaffected sides, respectively. $t_{affected,i}$ and $t_{normal,i}$ represent the *i*-th motion execution time of affected and unaffected side, respectively; N and M are the execution number of times of affected and unaffected side, respectively. Therefore, the indicator for the difference of motion execution time between affected and unaffected side could be defined as:

$$E_{time} = \frac{T_{r,affected}}{T_{r,normal}}, 0 \le E_{time} \le 1 \quad (23)$$

For this indicator, the larger E_{time} is, the smaller the difference of motion execution time between affected and unaffected side is.

After defining three indicators above, these indicators are possible to indicate the advancement of stroke patients on the aspect of motion angle, synergy and execution speed before and after rehabilitation.

4. Results and discussion

In this section, the measured inertial data from both healthy adults and stroke patients are employed to calculate the proposed three indicators. We relate WMFT scores to the indicators of subjects' inertial signals measured from shoulder flexion movement, and especially employ the least squares method to estimate the weightings of three indicators. The well-decided weightings make the proposed quantitative evaluation appropriately correlate with traditional rehab assessment scales. Thus, an individual rehab performance can be evaluated by an objective score that is the sum of three indicators multiplied by their weightings.

4.1. Indicators Analysis

4.1.1. Case 1: healthy adult

The person in this case is a normal healthy adult without upper limb diseases. Figure 6 shows the inertial signals of executing one period of motion on wrist, and the indicators are shown in Table 3. Notice that the dominant hand is viewed as unaffected side whereas the non-dominant hand as affected side in all indicators because there is no affected side for healthy people.

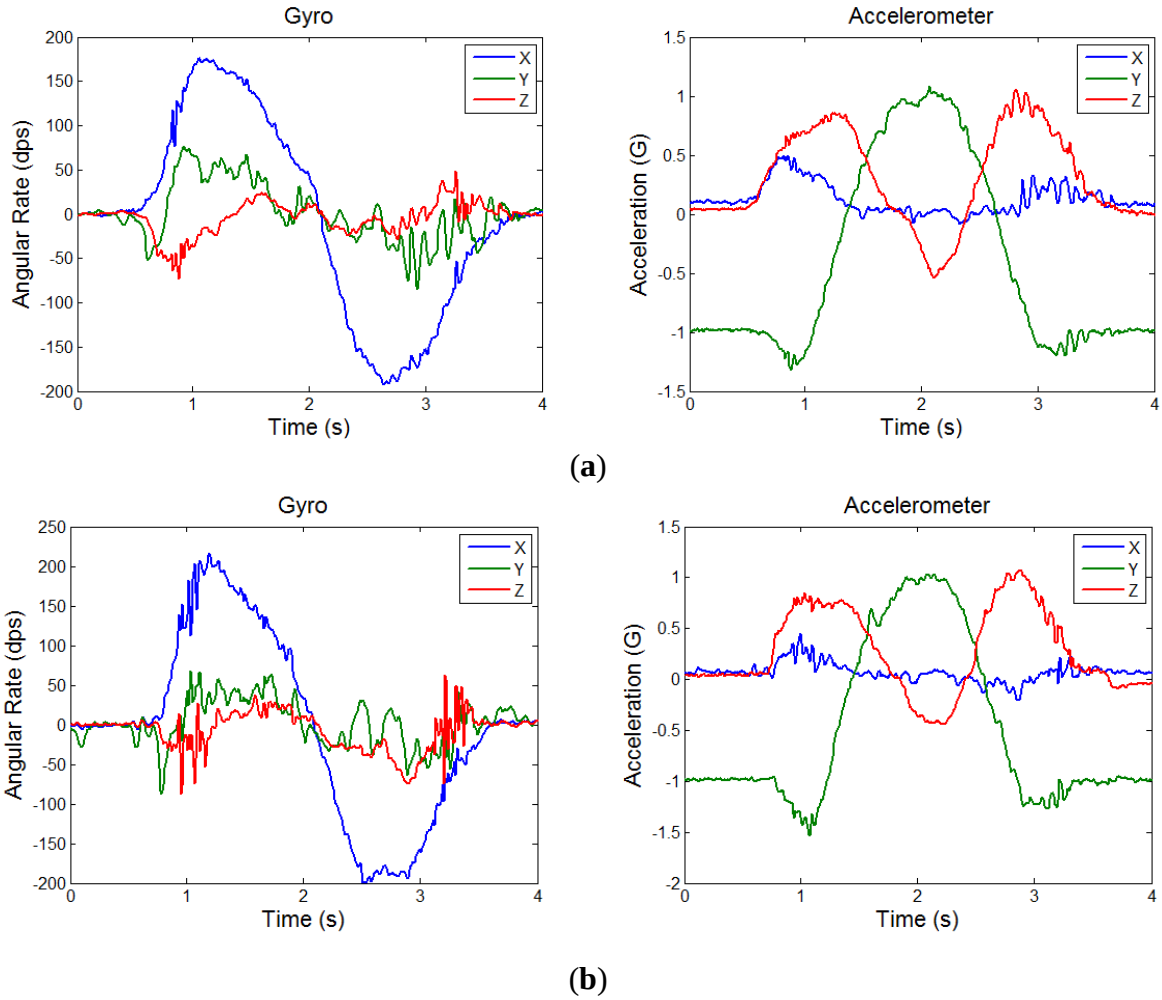

Figure 6. The inertial signals of executing the assessment motion of healthy adult on wrist. (**a**) The signals from dominant hand. (**b**) The signals from non-dominant hand.

Significant indicators	$A_{2,r}$	G_r	E_{time}
Scores	1.00	0.95	0.98

Table 3. The scores of indicators from case 1.

4.1.2. Case 2: stroke patient

The subjection in this case is a 68-year-old man with left side hemiplegia due to right thalamic intracerebral. The frequency of treatment is 3 times per week and once an hour with totally 24 hours. The inertial signals of pre-test (before treatment) and post-test (after treatment) with executing one period of motion on wrist from affected side are shown in Figure 7(a) and 7(b), respectively. The inertial signals of unaffected side test is shown in Figure 7(c).

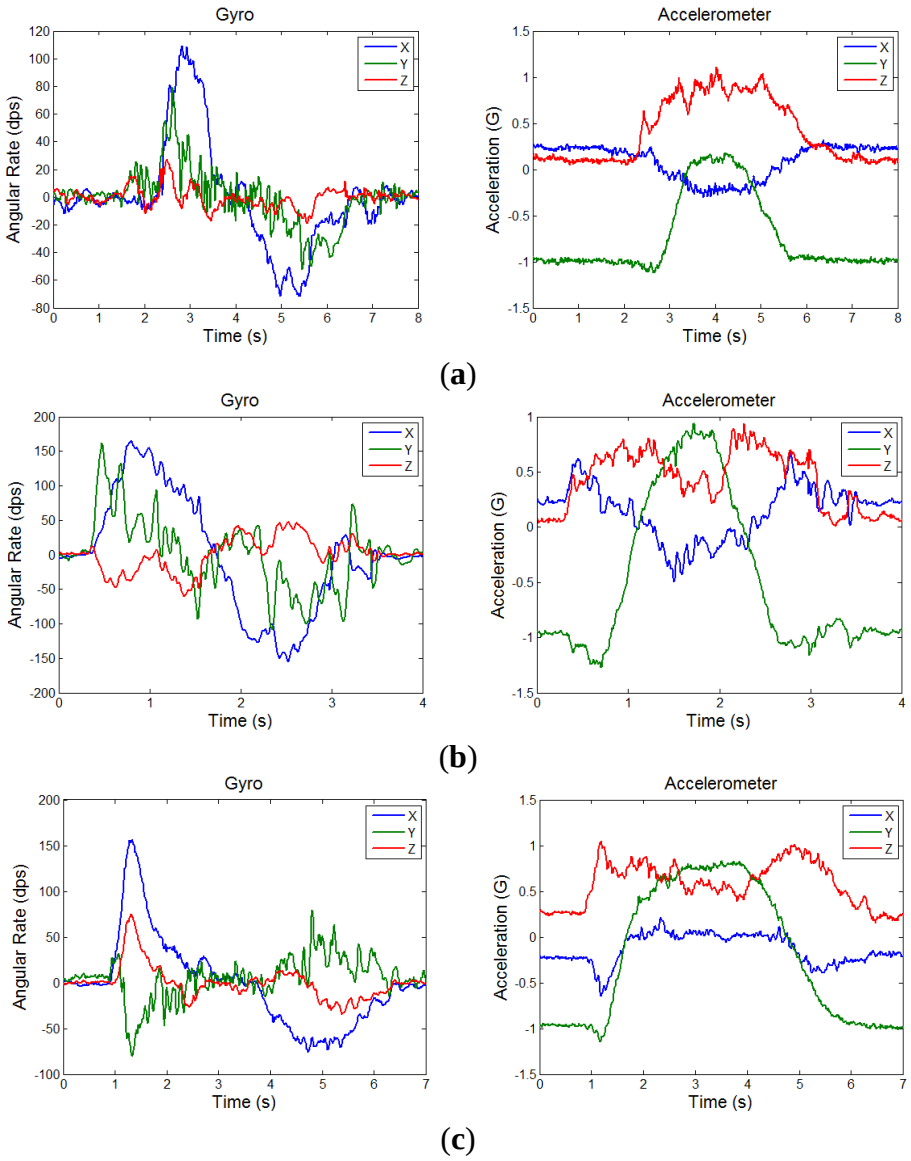

Figure 7. The inertial signals of executing the assessment motion of stroke patient on wrist. (**a**) The pretest signals from affected side. (**b**) The post-test signals from affected side. (**c**) The signals from unaffected side test.

Comparing the indicators of pre-test with post-test, we found that the Y-axis maximum acceleration at post-test is much approaching to +1 than pre-test. This means the arm at post-test were lifted higher than pre-test. On the aspect of angular velocity, although the X-axis value at post-test is much larger than the pre-test, the values in the others axis increased, too. This means that the synergy pattern became severer than the pre-test. The results of indicators are shown in Table 4. A reasonable reason that synergy indicators at both pre-test and post-test equal 1 because the unaffected test performed not well. This means the unaffected test executed with unnecessary movements, which resulted in the synergy indicators were overvalued. Overall, after rehabilitation treatment, this patient in case 2 actually improved his action ability, which can be observed from quantitative indicators.

4.2. Objective Evaluation Score

In this section, 1 healthy adult and 11 patients' assessment of both pre-test and post-test recorded data consist of WMFT score and three quantitative indicators will be used to employ the least squares meth od through linear regression. Therefore, the weights of three indicators, and the objective evaluation score defined as below will be obtained, i.e.

$$Q = 100 \times (\alpha \times A_{2,r} + \beta \times G_r + \gamma \times E_{time}), \tag{24}$$

where the indicators were defined in Eqs. (18), (21) and (23); α, β, γ represent the weights of indicators. The range of objective evaluation score Q is between 0 and 100.

Due to the summation of weights for indicators equal 1, (24) can be rewritten to Eq. (25):

$$Q = 100 \times [(1 - \beta - \gamma)] \times A_{2,r} + \beta \times G_r + \gamma \times E_{time}). \tag{25}$$

We have the sample data $(A_{2,r,1}, G_{r,1}, E_{time,1}, Q_1), (A_{2,r,2}, G_{r,2}, E_{time,2}, Q_2), \ldots,$ and $(A_{2,r,n}, G_{r,n}, E_{time,n}, Q_n)$, and thus

$$\frac{Q_i}{100} = A_{2,r} + \left(G_r - A_{2,r}\right) \times \beta + \left(E_{time} - A_{2,r}\right) \times \gamma + \varepsilon_i \text{ , i} = 1,2, \ldots, \text{n.} \tag{26}$$

where $\varepsilon_i = \frac{Q_i}{100} - \frac{\tilde{Q}_i}{100}$ is the error between the real value and the estimated value. To solve the linear regression, the least squares method was employed to have

$$L = \sum_{i=1}^{n} {\varepsilon_i}^2 = \sum_{i=1}^{n} \left[\frac{Q_i}{100} - A_{2,r} - \left(G_r - A_{2,r}\right) \times \beta - \left(E_{time} - A_{2,r}\right) \times \gamma\right]^2. \tag{27}$$

Solving β and γ through linear regression for a minimum L results in

$$\begin{aligned} \left.\frac{\partial L}{\partial \beta}\right|_{\hat{\beta},\hat{\gamma}} &= -2\sum_{i=1}^{n}\left[\frac{Q_i}{100} - A_{2,r} - \left(G_r - A_{2,r}\right) \times \hat{\beta} - \left(E_{time} - A_{2,r}\right) \times \hat{\gamma}\right]\left(G_r - A_{2,r}\right) = 0, \\ \left.\frac{\partial L}{\partial \gamma}\right|_{\hat{\beta},\hat{\gamma}} &= -2\sum_{i=1}^{n}\left[\frac{Q_i}{100} - A_{2,r} - \left(G_r - A_{2,r}\right) \times \hat{\beta} - \left(E_{time} - A_{2,r}\right) \times \hat{\gamma}\right]\left(E_{time} - A_{2,r}\right) = 0. \end{aligned} \tag{28}$$

Then we obtain

$$\begin{aligned} &\textstyle\sum_{i=1}^{n} A_{2,r}\left(G_r - A_{2,r}\right) + \hat{\beta} \times \sum_{i=1}^{n}\left(G_r - A_{2,r}\right)^2 + \hat{\gamma} \times \sum_{i=1}^{n}\left(E_{time} - A_{2,r}\right)\left(G_r - A_{2,r}\right) = \frac{1}{100}\sum_{i=1}^{n} Q_i\left(G_r - A_{2,r}\right), \\ &\sum_{i=1}^{n} A_{2,r}\left(E_{time} - A_{2,r}\right) + \hat{\beta} \times \sum_{i=1}^{n}\left(G_r - A_{2,r}\right)\left(E_{time} - A_{2,r}\right) + \hat{\gamma} \times \sum_{i=1}^{n}\left(E_{time} - A_{2,r}\right)^2 = \frac{1}{100}\sum_{i=1}^{n} Q_i\left(E_{time} - A_{2,r}\right) \end{aligned} \tag{29}$$

In statistics, we take the shoulder-related actions (which contained forearm to table. forearm to box, hand to table, hand to box, lift can, and lift basket) in WMFT scale scores as Q_i value in Eq. (29). The patients' scores of shoulder-related actions in WMFT are shown in Table 5. Because of the different scales of WMFT scale and objective evaluation score, it is necessary to adjust WMFT scale as

$$WMFT_{score} = \frac{WMFT_{raw}}{WMFT_{total}} \times 100, \tag{30}$$

where $WMFT_{raw}$ is patient's score of shoulder-related actions in WMFT and $WMFT_{total}$ is the total score of shoulder-related actions in WMFT.

To solve Eq. (29), we substitute three indicators and the adjusted WMFT scores to Eq. (29). As a result, the weights of indicators will be acquired. After we have the weights of indicators, the quantitative and objective evaluation score can be renew as Eq. (31), and the results are shown in Table 6, where case 12 is the healthy adult.

$$Q = 100 \times (0.20 \times A_{2,r} + 0.72 \times G_r + 0.08 \times E_{time}) \tag{31}$$

To investigate the correlation between the proposed quantitative evaluation method and traditional rehabilitation assessment scales, the scores of objective evaluation and items related to shoulder in WMFT are used to apply linear regression demonstrated as Figure 8. The coefficient of determination R^2 0.52 partly results from not enough samples. To improve the coefficient of determination, more relevant data need to be collected in the future such that the regression line will be closer to the scores.

Significant indicators	$A_{2,r}$	G_r	E_{time}
Pre-test	0.60	1.00	0.67
Post-test	1.00	1.00	0.88

Table 4. The scores of indicators from case 2.

Case	Pre-test	Post-test	Case	Pre-test	Post-test
1	25	24	**7**	8	15
2	9	12	**8**	20	25
3	19	19	**9**	21	23
4	20	22	**10**	9	12
5	20	24	**11**	11	17
6	13	17			

Table 5. Scores of shoulder-related actions in WM FT for stroke patients.

Case	$A_{2,mr}$		G_{rr}		E_{time}		Q	
	Pre-test	**Post-test**	**Pre-test**	**Post-test**	**Pre-test**	**Post-test**	**Pre-test**	**Post-test**
1	0.60	1.00	1.00	1.00	0.67	0.88	90	99
2	0.39	0.51	0.34	0.42	0.19	0.28	33	42
3	0.50	0.63	0.82	0.84	0.28	0.35	71	76
4	1.00	1.00	0.58	0.61	0.83	0.83	68	70
5	0.34	0.39	0.57	0.63	0.34	0.48	51	57
6	0.52	0.69	0.76	0.73	0.48	0.43	69	69
7	0.49	0.74	0.41	0.49	0.31	0.60	41	54
8	0.48	0.64	0.61	0.64	0.35	0.51	56	63
9	0.38	0.59	0.53	0.53	0.20	0.34	47	52
10	0.43	0.49	0.38	0.39	0.64	0.68	41	44
11	0.43	0.53	0.37	0.41	0.25	0.46	37	44
12	1.00		0.95		0.98		96	

Table 6. Results of objective evaluation score for stroke patients.

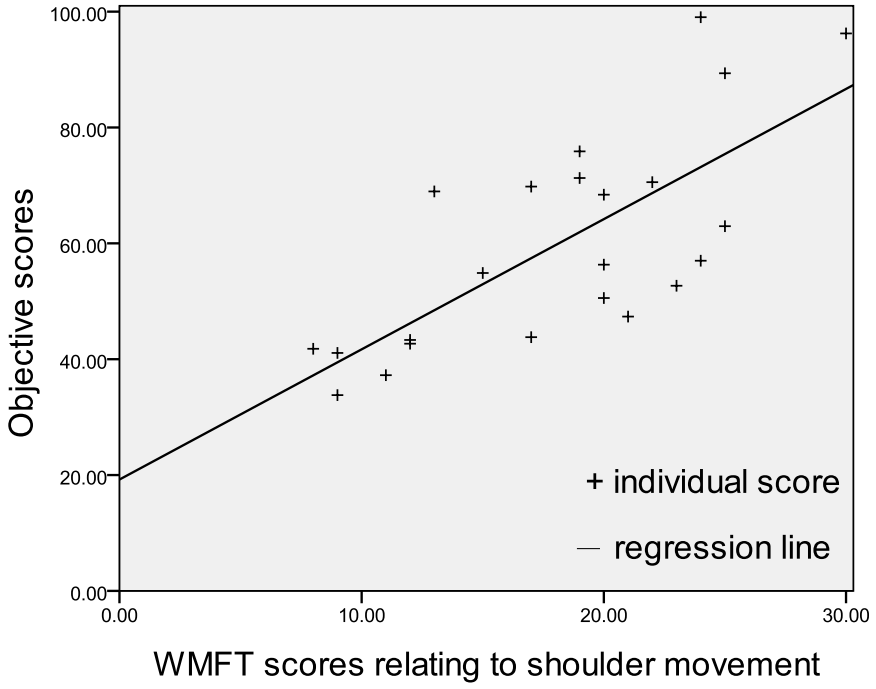

Figure 8. Linear regression between objective scores and WMFT scores relating to shoulder flexion.

5. Conclusion

In short, this study establishes a set of wireless inertial sensing system and enables to measure the inertial sensing signals from upper extremity. Additionally, the introduced evaluation method appears to have the potential to overcome some of the shortcomings of traditional assessment methods and indicate post-stroke rehab performance correctly. To correlate the objective evaluation indicators with the traditional assessment scales, the study first proposed determining the weighting corresponding to each

indicator by using the least squares method. From the clinical trial results, it shows acquiring more experimental data are needed to improve the coefficient of determination.

Acknowledgments

This work was partially supported by the VGHUST Joint Research Program, Tsou's Foundation under grants VGHUST100-G4-1-2 and VGHUST102-G4-1-1. The funding is gratefully acknowledged.

Conflicts of Interest

The authors declare no conflict of interest.

References and Notes

1. "The top l 0 causes of death", World Health Organization, 2014.
2. V. L. Feigin, M. H. Forouzanfar, R. Krishnamurthi, G. A. Mensah, M. Connor, D. A. Bennett, A. E. Moran, R. L. Sacco, L. Anderson, T. Truelsen, M. O'Donnell, N. Venketasubramanian, S. Barker-Collo, C. M. Lawes, W. Wang, Y. Shinohara, E. Witt, M. Ezzati, M. Naghavi, C. Murray, "Global and regional burden of stroke during 1990-2010: findings from the Global Burden of Disease Study 2010." Lancet 383 (9913): 245-254, 2014.
3. C. E. Coffey, J. L. Cummings, S. Starkstein, R. Robinson, ·"Stroke - the American Psychiatric Press Textbook of Geriatric Neuropsychiatry," 2nd Ed., Washington DC: American Psychiatric Press, pp. 601 - 617, 2000.
4. N Gordon, M Gulanick, F Costa, G Fletcher, B Franklin, E Roth, T Shephard, "Physical activity and exercise recommendations for stroke survivors," Circulation vol. I 09, pp. 2031 - 2041, 2004.
5. A. Fugl-Meyer, L. Jaasko, I. Leyman, S. Olsson, and S. Steglind, "The post-stroke hemiplegic patient. 1. a method for evaluation of physical performance," Scandinavian Journal of Rehabilitation Medicine, vol. 7. no. 1, pp. 13- 31, 1975.
6. S. L. Wolf, P. A. Catlin, M. Ellis, A. L. Archer, B. Morgan, and A. Piacentino, "Assessing Wolf Motor Function Test as Outcome Measure for Research in Patients After Stroke," Stroke, vol. 32, no. 7, pp. 1635- 1639, 2001.
7. J. Desrosiers, R. Hebert, E. Dutil, and G. Bravo, "Development and Reliability of an Upper Extremity Function Test for the Elderly: The TEMPA," Canadian Journal of Occupational Therapy, vol. 60, no. 1, pp. 9-16, 1993.
8. S. Allin, N. Baker, E. Eckel, D. Ramanan, "Robust Tracking of the Upper Limb for Functional Stroke Assessment," IEEE Trans on Neur. Sys. and Rehab. Eng., vol. 18, no. 5, pp. 542-550, 2010.
9. D. Pang, C. Nessler, J. Painter, and C. Reinkensmeyer, "Web-based telerehabilitation for the upper extremity after stroke," IEEE Trans on Neur. Sys. and Rehab. Eng., vol. 10, pp. 2102–2108, 2002.
10. M. Goffredo, I. Bernabucci, M. Schmid, and S. Conforto, "A neural tracking and motor control approach to improve rehabilitation of upper limb movement," J. NeuroEng and Rehab, vol. 5, no. 5, 2008.

11. M. Woodbury, D. Howland, T. McGuirk, S. Davis, C. Senesac, S. Kautz, and L. Richards, "Effects of trunk restraint combined with intensive task practice on post-stroke upper extremity reach and function," Neurorehabil Neural Repair, vol. 23, no. 1, pp. 78–91, 2009.
12. E. M. C. Hillman, J.C. Hebden, M. Scheiger, H. Dehghani, F. E.W. Schmidt D. T. Delpy, S. R. Arridge, "Time resolved optical tomography of the human forearm," Physics in Medicine and Biology, vol. 46, no. 4, pp. 1117- 1130, 2001.
13. H. Zheng, N.D. Black, and N.D. Harris, "Position-Sensing Technologies for Movement Analysis in Stroke Rehabilitation," Medical & Biological Engineering & Computing, vol. 43, pp. 413-420, 2005.
14. J. Kim, S. Yang, and M. Gerla, "StrokeTrack: Wireless Inertial Motion Tracking of Human Arms for Stroke Telerehabilitation," mHealthSys'11, no. 4, 2011.
15. H. Zhou, H. Hu, Y. Tao. "Inertial measurements of upper limb motion," Medical & Biological Engineering & Computing, vol. 44, pp. 479-487, 2006.
16. B. Hingtgen, J. R. McGuire, M. Wang, G. F. Harris, "An upper extremity kinematic model for evaluation of hemiparetic stroke," Journal of Biomechanics, vol. 39, no. 4, pp. 681-688, 2006.
17. InvenSense, "MPU-6050 Product Specification Rev 3.3."
18. Asahi KASEI, "AK8975 Electronic Compass."
19. H. Labiod, H. Afifi, C. De Santis, "Wi-Fi™, Bluetooth™, ZigBee™, and WiMax™," Springer, 2007.
20. "XBee/XBee-Pro RF Modules Product Manual." DIGI, 2012.
21. M. S. Grewal, L. R. Weill, and A. P. Andrews, "Global Positioning Systems, Inertial Navigation, and Integration," 2nd Ed., Wiley-Interscience, 2007.
22. C. Konvalin, "Compensating for Tilt, Hard Iron, and Soft Iron Effects," Rev 1.2, MEMSense, 2008.
23. W. T. Fong, S. K. Ong, and A. Y. C. Nee, "Methods for in-field user calibration of an inertial measurement unit without external equipment," Measurement Science and Technology, vol. 19, no. 8, 085202, 2008.
24. G. Thrane, N. Emaus, T. Askim, and A. Anke, "Arm Use in Patients with Subacute Stroke Monitored by Accelerometry: Association with Motor Impairment and Influence on Self-Dependence," Journal of Rehabilitation Medicine, vol. 43, no. 4, pp. 299- 304, 2011.